Bifurcation and hyperchaos from a class B tri-laser system

Sen-Lin Yan(颜森林), Hai-Jun Wang(王海军)
Citation: Chin. Phys. B. 35, 100501 (2026). DOI: 10.1088/1674-1056/ae3b2e | CSTR: 32038.14.CPB.ae3b2e
http://cpb.iphy.ac.cn; http://iopscience.iop.org/cpb

What follows is a list of articles you may be interested in

A novel three-dimensional chaotic system with double wings and spiral chaos: Applications in ship radiation noise detection

Hong Yang(杨宏), Shijia Wang(王世佳), Guohui Li(李国辉)
Chin. Phys. B. 35, 090506 (2026). DOI: 10.1088/1674-1056/ae111c | CSTR: 32038.14.CPB.ae111c

Coupling-induced dynamics in a stochastic two-predator two-prey system with Markov switching

Ya-Nan Sun(孙雅楠), Xin-Zhi Liu(刘新芝), You-Ming Lei(雷佑铭)
Chin. Phys. B. 35, 080507 (2026). DOI: 10.1088/1674-1056/ae8daf | CSTR: 32038.14.CPB.ae8daf

Multistability and offset boosting in a fractional-order discrete memristive neuron model with application to image encryption

Haneche Nabil, Hamaizia Tayeb
Chin. Phys. B. 35, 080504 (2026). DOI: 10.1088/1674-1056/ae1454 | CSTR: 32038.14.CPB.ae1454

A modular-bias-sin chaotification method for enhanced discrete memristor chaotic maps

Shu Yi(易澍), Huihai Wang(王会海), Kehui Sun(孙克辉)
Chin. Phys. B. 35, 070504 (2026). DOI: 10.1088/1674-1056/ae181e | CSTR: 32038.14.CPB.ae181e

Symmetrical Turing instability in Chua corsage memristor siblings-based two-cell network

Zhicheng Tian(田桎成), Peipei Jin(靳培培), Shutong Liu(刘姝彤), Meiyuan Gu(顾梅园), Long Chen(陈龙), Guangyi Wang(王光义)
Chin. Phys. B. 35, 060511 (2026). DOI: 10.1088/1674-1056/ae68f9 | CSTR: 32038.14.CPB.ae68f9

Bifurcation and hyperchaos from a class B tri-laser system

Sen-Lin Yan(颜森林)[†] and Hai-Jun Wang(王海军)

School of Electronic Engineering, Nanjing Xiaozhuang University, Nanjing 210017, *China*

(Received 16 October 2025; revised manuscript received 19 January 2026; accepted manuscript online 21 January 2026)

This paper presents a novel delayed double-ring anti-phase-coupling class B tri-laser system. Subsequently, this work creates a hyperchaotic laser transmitter, after which it provides a comprehensive analysis of its theoretical model, including six infinite-dimension rate equation sets and corresponding numeric results. We qualitatively investigate the dynamic behaviors, including the existence and stability of steady states, as well as the occurrence and suppression of bifurcation, chaos, and hyperchaos. We expound on how both delayed time and anti-phase-coupling effects influence the tri-laser system's behavior and lead to chaotic and hyperchaotic phenomena. We also analyze instability and multi-stability according to the nonlinear function in theory and find that multi-stability exists in an unstable region. The investigation of the tri-laser configuration provides insights into the tri-laser structure that plays a special role in the chaotic system. Simultaneously, our numeric simulation demonstrates the existence of instability via a typical nonlinear curve diagram and the existence of multi-stability via a set of quasiperiodic attractors. The system exhibits a rich variety of nonlinear dynamic behaviors, including hyperchaos, chaos, period 1, period 3, and coexistent scenarios, and following a route to chaos via bifurcation. The corresponding dynamics are identified and characterized using Lyapunov exponents. Chaos control is successfully achieved, yielding quasiperiods such as periods 3, 6, and 12, thereby steering the system away from chaos. The results provide valuable references for the study of chaotic transmitters, laser technology, hyperchaos, and their applications.

Keywords: chaos, bifurcation, class B laser, control

PACS: 05.45.–a, 05.45.Gg, 05.45.Pq, 42.55.–f

DOI: 10.1088/1674-1056/ae3b2e **CSTR:** 32038.14.CPB.ae3b2e

1. Introduction

To describe laser chaos, Haken discovered well-known Maxwell–Bloch equation sets. This great finding considerably encouraged laser, optical, and chaos communities to explore fascinating nonlinear dynamic behaviors, including laser chaos in class A, class B, and class C laser systems, along with their applications.[1–5] Recently, in optics and laser physics, the class B laser system followed rotating wave theory and considered only the variety of electric field and population inversions inside the laser. It exhibits typical nonlinear dynamic phenomena, such as unsteady states, bifurcations, stochastic oscillations, and chaos, using additional dimension technology.[6–10] Due to a chaotic signal characterized by a flat broadband spectrum and randomness, its attractor is characterized by ergodicity.[11–14] Hence, laser chaos exhibits unforecasted dynamic behavior.[15–17] As class B laser chaos devices, such as the semiconductor laser and fiber laser, a chaotic semiconductor laser has the characteristics of a tiny size, a model block, a short oscillation time, and easy production. A chaotic fiber laser is characterized by fibers that fuse readily with communication systems. Thus, chaotic lasers have been created to be widely adopted for high-speed chaotic optical communications, analog optical computing, fine measuring instruments, and optical random number generators.[4–7] Therefore, the class B laser is an ideal candidate for the study of optical chaotic systems and their applications.

The existence of chaos in a dynamic system is associated with its one positive Lyapunov exponent (LE). A hyperchaotic existence is linked with at least two positive LEs. However, many chaotic lasers contain only one positive LE. A hyperchaotic laser system is difficult to produce to a certain extent. Nonetheless, with the development of chaotic laser technology, hyperchaos has continuously been reported in free-running lasers, Zeeman lasers, double-ring Er-doped fiber lasers, and three-ring Er-doped fiber lasers.[2,3] Research on hyperchaotic laser systems has become a hot topic in chaos and laser physics. Correspondingly, we were motivated to study hyperchaotic lasers.

Many types of coupled lasers have recently been reported in both experiments and theory, including the double-ring coupled Er-doped fiber laser and the two coupled semiconductor lasers. Such coupled lasers readily produce two chaotic signals.[18–20]

Coupled laser systems have found broad application in the optics and photoelectron fields, such as in high-frequency generators, secure communications, radars, sensors, and random signal generators that use chaotic signals. Previous studies have investigated the dynamics of two coupled lasers.[21–23] After our analysis of those coupled-laser systems,[24–26] we found that two active sources (or lasers) re-

[†]Corresponding author. E-mail: senlinyan@163.com

© 2026 Chinese Physical Society and IOP Publishing Ltd. All rights, including for text and data mining, AI training, and similar technologies, are reserved.

sult in recurrent action among two field intensities and phases inside the two subsystems, mainly leading to a quasiperiodic breakdown to chaos. To create a novel type of laser hyperchaos transmitter,[27] this work developed two-coupled laser technology as a new delayed double-ring anti-phase coupling technology. With it, we presented a hyperchaotic tri-laser system comprising three single class B lasers, where the delayed double-ring anti-phase coupling operation causes both the effects of the time delay and anti-phase coupling on the dynamics of three subsystem lasers. Three active sources resulted in recurrent action among the electric fields inside the three subsystems, leading to a nonlinear dynamic process, with a quasiperiodic breakdown into chaos and hyperchaos occurring in the system.

Because the tri-laser system has more complex nonlinear interactions than the double-coupled laser system, the tri-laser system is theoretically expected to exhibit more diverse dynamic behaviors than the double-coupled laser system. The dynamics caused by the delayed time and anti-phase-coupling operation are highly complex, even if the independent (uncoupled) unit maintains a stable equilibrium. Therefore, research on coupling multi-laser structures has great value for the development of coupled oscillators, laser systems, complex systems, and optical chaos. Nonetheless, a comprehensive investigation is still necessary and significant to analyze the dynamics of various coupling multi-laser configurations.

Furthermore, multi-stability, which denotes the coexistence of multiple stable states or quasiperiodic attractors inside a parameter region, is an intriguing phenomenon.[28,29] Accordingly, we also discuss the multi-stability of the tri-laser system.

Chaos in lasers has been found to demonstrate only a single-scroll chaotic attractor or a double-scroll chaotic attractor in dynamic phase space. Consequently, creating a new type of chaotic attractor or a multi-scroll chaotic attractor displayed in a dynamic phase space is a topic of considerable interest. After examining many multi-scroll chaotic attractors, it was found that some often possess hyperchaotic characteristics.[3,30] Hyperchaotic systems and their multi-scroll hyperchaotic attractors have aroused great interest because hyperchaotic systems can enhance the security of chaotic coding by utilizing hyperchaotic signals.

By studying the tri-laser system, it was found that this system has two positive LEs and reveals multi-scroll hyperchaotic attractors. From an application perspective, if this hyperchaotic system were employed for secure communication, it would be exceedingly difficult for intruders to predict the dynamic behavior of the system. Therefore, the system's hyperchaotic signal can augment the security of chaotic coding.

From the standpoint of spatial dynamics, this architecture is accomplished by realistically modeling spatially extended systems because the dominant features of the underlying laser constituents are retained. Such a built-up device creates a novel laser system whose dynamic behavior is richer than a single laser or two coupled lasers, yet remains analytically tractable. From a control standpoint, delayed coupling technology readily allows adjustment of delay times and coupling levels to guide a system's dynamic behavior and control chaos.[29,31,32] maintaining controllability.

Chaos control is another important issue.[31–33] Chaos control indicates that a chaotic movement can be suppressed to reduce it to a quasi-periodic state or a stable state. Since the Ott, Grebogi and Yorke (OGY) method of chaos control was proposed, numerous chaos control methods have been presented, such as weak periodic perturbation, continuous feedback, nonlinear feedback, multiple-parameter, and adaptive control.[31–33] We will research the chaotic control of the three-laser system to reveal hidden behavior. The control of a chaotic multi-laser system is also meaningful work because many previous studies have focused on the chaotic control of single-laser systems.

In optics and laser physics, class B lasers encompass various types, including semiconductor and fiber lasers. Therefore, the proposed system holds broad representativeness within the optics and laser fields. The research advantages of this system also indicate that our simplified model can overlook the structure and coefficients of specific class B lasers, thereby avoiding the examination of many parameters. We inspected only the influence of the coupling level and the delay time on system dynamics through a set of six infinite-dimension normalized rate equations. Our analysis offers a deeper understanding of the stochastic behavior of the tri-laser system.

We present our research question and concept as follows: Does nonlinear dynamics such as instability, stability, and multi-stability exist? How does the system produce chaos and hyperchaos? What is the impact of motivation on instability, stability, and multi-stability when anti-phase coupling is operated? How do time delays influence instability and stability? What are the dynamics when anti-phase coupling and time delays are simultaneously operated? Will dynamic behaviors, such as period 1, chaos, hyperchaos, etc., be displayed due to these effects? How do we analyze the infinite-dimension tri-laser system, and how does its distinct feature display in the tri-body problem (compared with the infinite-dimension single-laser system or two-laser system)? How do we reveal the hidden behavior of the system? Accordingly, we were motivated to discern how anti-phase coupling and delayed time feedback jointly affected stability, chaos, and the existence of other dynamics that could not be displayed in the traditional single laser-delayed system and the two coupled laser system.

Interestingly, the tri-laser system behaves as if it has no

ends, no rules, or randomness, which has great value in revealing the hidden behavior of a multi-body case in physics. Our work has significant reference value for studying how to create a hyperchaotic transmitter, class B laser, laser technology, nonlinear optics, and their applications.[22–26,35–38]

The stability theory of mathematics is typically used to analyze the stability of dynamic systems described by differential equations of degree four or lower. Because there is no root formula for polynomials of the fifth order or above, we restrict our study to qualitative dynamic behaviors using the stability theory. However, we adopted nonlinear function theory to reveal the instability of the system. Our research revealed the stability of the three-laser system described by differential equations of degree six and the occurrence of bifurcation phenomena. Thereby, our research is contributing to the study of dynamic systems described by differential equations of degree five or more.

This paper is organized as follows. In Section 2, we present the system's model. In Section 3, we conduct a qualitative analysis of the stability, bifurcation, instability, and multi-stability of the two theories of perturbation and function and investigate the existence of strange attractors and quasi-periodic attractors. In Section 4, we numerically illustrate instability, provide a route to hyperchaos, operate chaos control, and analyze system dynamics via the LE spectrum. Finally, Section 5 presents our conclusion.

2. Configuration and theory

In both optics and laser physics, the well-known three-dimensional Maxwell–Bloch equations can be simplified to two-dimensional forms to describe the dynamics of single-mode uniformly broadened traveling-wave lasers. To create a novel tri-laser system scheme (cf. Fig. 1), we present a delayed anti-phase-coupling class B three-laser system, forming a double-ring-coupling configuration. Optical paths are introduced. One optic ring path consists of lasers 2, 3, 1, and anti-phase coupler (APC). Another optic ring path comprises lasers 2, 1, and an APC. Two sets of lasing from

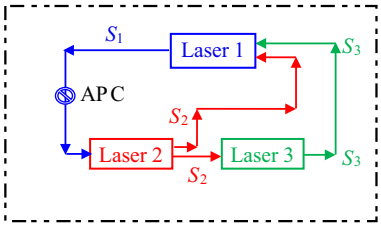

Fig. 1. Schematic of delayed double-ring anti-phase-coupling B-class three-laser system. S represents the field. APC is an anti-phase coupler.

Lasers 2 and 3, respectively, were injected into lasers 1 and 3. The lasing from laser 3 was injected into laser 1, which results in the enhancement of the oscillation of double-injection laser 1. The lasing from laser 1 was anti-phase injected into laser 2 to compress its oscillation. Due to the existence of a delayed time, this performance resulted in the alternative compression and enhancement of the oscillations of neighboring lasers and led to dynamic changes to each laser. Last, such an operation may cause the system's multi-stability or instability. The laser physics model of the system is introduced via three sets of two-dimensional Maxwell–Bloch equations to describe the electric fields and the population inversions inside the three lasers. Considering the delayed time, the model is described using a set of infinite-dimensional normalized rate equations, as follows:[22–26]

$$\mathrm{d}S_1/\mathrm{d}t = -a_1[S_1 - m_1 S_2(t-\tau) - m_1 S_3(t-\tau)] + a_1 S_1 D_1, \quad (1)$$

$$\mathrm{d}D_1/\mathrm{d}t = \sigma_1(R_1 - D_1) - S_1^2 D_1, \quad (2)$$

$$\mathrm{d}S_2/\mathrm{d}t = -a_2[S_2 + m_2 S_1(t-\tau)] + a_2 S_2 D_2, \quad (3)$$

$$\mathrm{d}D_2/\mathrm{d}t = \sigma_2(R_2 - D_2) - S_2^2 D_2, \quad (4)$$

$$\mathrm{d}S_3/\mathrm{d}t = -a_3[S_3 - m_3 S_2(t-\tau)] + a_3 S_3 D_3, \quad (5)$$

$$\mathrm{d}D_3/\mathrm{d}t = \sigma_3(R_3 - D_3) - S_3^2 D_3. \quad (6)$$

The footnotes "1, 2, and 3" indicate each laser. S is the electric field. D is the population inversion in the laser. The coefficient $a = k/\delta$ is the ratio of the cavity loss k to the longitudinal relaxation constant δ. The coefficient $\sigma = r/\delta$ is the ratio of the longitudinal relaxation constant to the transverse relaxation constant r. R represents the pump rate of each laser, and the pump level dominates the laser's output. In addition, τ is the delayed time, and parameter m is the coupling coefficient, indicating the injection level of light from one laser to another or representing the coupling level of the system. In practice, the value m can be adjusted with optic amplifiers and optic attenuators. The value k can be adjusted with an additional absorber.

3. Theory of stability and Hopf bifurcation

3.1. Perturbation theory

Because there is no root formula for a triquadratic form, we focus on qualitative analysis of dynamic behaviors, including the existence of a steady state, its stability, the occurrence and forbiddance of bifurcation, and delayed performance.

We found that delayed time cannot change equilibrium points. However, it can alter the dynamic behavior of each laser in real time. Our study of the linear stability of equilibrium points will investigate the root distribution of the following transcendental equation, describing a characteristic equation. We adopt an approximation as follows:

$$S_i(t) = S_{i0} + \delta S_i, \quad D_i(t) = D_{i0} + \delta D_i,$$

where $i = 1$, 2, and 3, footnote "0" indicates the equilibrium points of each laser and substitutes them into Eqs. (1)–(6).

After the linearization of the tri-laser system, a perturbation equation describing the stability of the equilibrium points is obtained with the following equation:

$$\frac{\mathrm{d}}{\mathrm{d}t}\begin{pmatrix}\delta S_1\\ \delta D_1\\ \delta S_2\\ \delta D_2\\ \delta S_3\\ \delta D_3\end{pmatrix}=\begin{pmatrix}A_{11}&A_{12}&A_{13}&0&A_{15}&0\\ A_{21}&A_{22}&0&0&0&0\\ A_{31}&0&A_{33}&A_{34}&0&0\\ 0&0&A_{43}&A_{44}&0&0\\ 0&0&A_{53}&0&A_{55}&A_{56}\\ 0&0&0&0&A_{65}&A_{66}\end{pmatrix}\begin{pmatrix}\delta S_1\\ \delta D_1\\ \delta S_2\\ \delta D_2\\ \delta S_3\\ \delta D_3\end{pmatrix}, \quad (7)$$

with

$$\begin{aligned}
&A_{11}=-a_1+a_1D_{10},\quad A_{12}=a_1S_{10},\\
&A_{13}=a_1m_1\,\mathrm{e}^{-\lambda\tau},\quad A_{15}=a_1m_1\,\mathrm{e}^{-\lambda\tau};\\
&A_{21}=-2D_{10}S_{10},\quad A_{22}=-\sigma_1-S_{10}^2;\\
&A_{31}=-a_2m_2\,\mathrm{e}^{-\lambda\tau},\quad A_{33}=-a_2+a_2D_{20},\quad A_{34}=a_2S_{20};\\
&A_{43}=-2S_{20}D_{20},\quad A_{44}=-\sigma_2-S_{20}^2;\\
&A_{53}=a_3m_3\,\mathrm{e}^{-\lambda\tau},\quad A_{55}=-a_3+a_3D_{30},\quad A_{56}=a_3S_{30};\\
&A_{65}=-2S_{30}D_{30},\quad A_{66}=-\sigma_3-S_{30}^2.
\end{aligned}$$

where λ is the characteristic value. The characteristic equation is given by

$$\begin{vmatrix}A_{11}-\lambda&A_{12}&A_{13}&0&A_{15}&0\\ A_{21}&A_{22}-\lambda&0&0&0&0\\ A_{31}&0&A_{33}-\lambda&A_{34}&0&0\\ 0&0&A_{43}&A_{44}-\lambda&0&0\\ 0&0&A_{53}&0&A_{55}-\lambda&A_{56}\\ 0&0&0&0&A_{65}&A_{66}-\lambda\end{vmatrix}=0. \quad (8a)$$

Equation (8a) is obviously a transcendental equation due to the term $\exp(-\lambda\tau)$. It is also written as follows:

$$\begin{aligned}
&(A_{66}-\lambda)(A_{55}-\lambda)(A_{44}-\lambda)(A_{33}-\lambda)(A_{22}-\lambda)(A_{11}-\lambda)\\
&-(A_{66}-\lambda)(A_{55}-\lambda)(A_{44}-\lambda)(A_{33}-\lambda)\\
&\times[(A_{11}-\lambda)A_{21}A_{12}+(A_{22}-\lambda)A_{31}A_{13}]\\
&-(A_{66}-\lambda)(A_{55}-\lambda)(A_{22}-\lambda)(A_{11}-\lambda)A_{34}A_{43}\\
&-(A_{44}-\lambda)(A_{33}-\lambda)(A_{22}-\lambda)(A_{11}-\lambda)A_{34}A_{43}A_{56}A_{65}\\
&+(A_{66}-\lambda)(A_{44}-\lambda)(A_{22}-\lambda)A_{15}A_{53}A_{31}\\
&+(A_{66}-\lambda)(A_{55}-\lambda)A_{34}A_{43}A_{21}A_{12}\\
&-A_{56}A_{65}(A_{44}-\lambda)[(A_{33}-\lambda)A_{21}A_{12}+(A_{22}-\lambda)A_{31}A_{13}]\\
&+A_{56}A_{65}A_{34}A_{43}(A_{22}-\lambda)(A_{11}-\lambda)\\
&-A_{56}A_{65}A_{34}A_{43}A_{12}A_{21}=0. \quad (8b)
\end{aligned}$$

It is well known that the stability and bifurcation of equilibrium points can be diagnosed with the root λ of Eq. (8).

First, three cases are discussed as follows:

(i) In the case of a real λ, when $\lambda<0$, the equilibrium point is stable. When $\lambda>0$, the equilibrium points are unstable. We readily find the solution of $\lambda=0$. We obtained the following critical coupling strengths:

$$A_{66}A_{44}A_{22}(a_1m_1a_2m_2a_3m_3)-A_{66}A_{55}A_{44}A_{33}A_{22}(a_1m_1a_2m_2)+B_0=0, \quad (9a)$$

where the parameter item B_0 is readily obtained from Eq. (8b) or from the following Eq. (11). To simplify, with settings $a_1=a_2=a_2=a$ and $m_1=m_2=m_3=m$, the critical coupling strength m_c is obtained with the following equation:

$$A_{66}A_{44}A_{22}(a^3m_\mathrm{c}^3)-A_{66}A_{55}A_{44}A_{33}A_{22}(a^2m_\mathrm{c}^2)+B_0=0. \quad (9b)$$

We readily obtain the root of the critical coupling strength m_c and obtain the following result: The equilibrium points become stable when $m<m_\mathrm{c}$, with the assumption that no other instability perturbs the stable state and ultra-short delayed time. Moreover, Hopf bifurcation is suppressed. When a coupling strength larger than m_c is added, the system experiences undamped oscillation, or chaos.

(ii) In the case of a complex λ, when $\mathrm{Re}(\lambda)<0$, the equilibrium point is stable, while a damped oscillation operates in the system. When $\mathrm{Re}(\lambda)>0$, the equilibrium points are unstable while an undamped oscillation or a stochastic oscillation operates in the system.

(iii) In the case of an imaginary λ, bifurcation occurs. If $\mathrm{j}\omega$ $(\omega\neq0)$ is only the root of Eq. (8), the Hopf bifurcation point can be obtained. Equation (8) is inspected to reveal six pure imaginary solutions due to the existence of the complex exponential items $\exp(-2\omega\tau\mathrm{j})$ and $\exp(-3\omega\tau\mathrm{j})$. Once the value ω has been obtained, we suppose that Eq. (8) has six roots of ω_i, where $i=1$, 2, 3, 4, 5, and 6. From Eq. (8(b)), the critical delayed time $\tau(\omega_i)$ is attained with the following equation:

$$\begin{aligned}
&(A_{66}-\mathrm{j}\omega_i)(A_{55}-\mathrm{j}\omega_i)(A_{44}-\mathrm{j}\omega_i)\\
&\times(A_{33}-\mathrm{j}\omega_i)(A_{22}-\mathrm{j}\omega_i)(A_{11}-\mathrm{j}\omega_i)\\
&-(A_{66}-\mathrm{j}\omega_i\lambda)(A_{55}-\mathrm{j}\omega_i)(A_{44}-\mathrm{j}\omega_i)(A_{33}-\mathrm{j}\omega_i)\\
&\times[(A_{11}-\mathrm{j}\omega_i)A_{21}A_{12}+(A_{22}-\mathrm{j}\omega_i)a^2m^2\,\mathrm{e}^{-2\mathrm{j}\omega_i\tau}]\\
&-(A_{66}-\mathrm{j}\omega_i)(A_{55}-\mathrm{j}\omega_i)(A_{22}-\mathrm{j}\omega_i)(A_{11}-\mathrm{j}\omega_i)A_{34}A_{43}\\
&+(A_{66}-\mathrm{j}\omega_i)(A_{55}-\mathrm{j}\omega_i)A_{34}A_{43}A_{21}A_{12}\\
&+(A_{66}-\mathrm{j}\omega_i)(A_{44}-\mathrm{j}\omega_i)(A_{22}-\mathrm{j}\omega_i)a^3m^3\,\mathrm{e}^{-3\mathrm{j}\omega_i\tau}\\
&-A_{56}A_{65}(A_{44}-\mathrm{j}\omega_i)(A_{33}-\mathrm{j}\omega_i)\\
&\times(A_{22}-\mathrm{j}\omega_i)(A_{11}-\mathrm{j}\omega_i)A_{34}A_{43}\\
&-A_{56}A_{65}(A_{44}-\mathrm{j}\omega_i)[(A_{33}-\mathrm{j}\omega_i)\\
&\times A_{21}A_{12}+(A_{22}-\mathrm{j}\omega_i)A_{31}A_{13}]\\
&+A_{56}A_{65}A_{34}A_{43}(A_{22}-\mathrm{j}\omega_i)(A_{11}-\mathrm{j}\omega_i)\\
&-A_{56}A_{65}A_{34}A_{43}A_{12}A_{21}=0. \quad (10)
\end{aligned}$$

This implies that bifurcation occurs in the system and that bifurcation processes can be guided by different critical delayed times because there are different numerical solutions in the transcendental equation (10).

Second, Eq. (8b) is rewritten as another expression of the transcendental equation

$$\lambda^6 + c_5\lambda^5 + c_4\lambda^4 + c_3\lambda^3 + c_2\lambda^2 + c_1\lambda + c_0 = 0, \quad (11)$$

where

$$\begin{aligned}
c_5 &= -\big(A_{11}+A_{22}+A_{33}+A_{44}+A_{55}\\
&\quad +A_{66}-A_{12}A_{21}-A_{13}A_{31}\big),\\
c_4 &= \sum_{1\le i<j\le 6} A_{ii}A_{jj} - A_{12}A_{21}\left(A_{11}+A_{33}+A_{44}+A_{55}+A_{66}\right)\\
&\quad -A_{31}A_{13}\left(A_{22}+A_{33}+A_{44}+A_{55}+A_{66}\right)\\
&\quad -A_{34}A_{43} - A_{56}A_{65}A_{34}A_{43},\\
c_3 &= -\sum_{1\le i<j<k\le 6} A_{ii}A_{jj}A_{kk} + A_{12}A_{21}\sum_{\substack{1<i<j\\ i,j\in 1,3,4,5,6}} A_{ii}A_{jj}\\
&\quad +A_{31}A_{13}\sum_{\substack{1<i<j\\ i,j\in 2,3,4,5,6}} A_{ii}A_{jj} - A_{15}A_{53}A_{31}\\
&\quad +A_{34}A_{43}\left(A_{11}+A_{22}+A_{55}+A_{66}\right)\\
&\quad +A_{56}A_{65}A_{34}A_{43}\left(A_{11}+A_{22}+A_{33}+A_{44}\right),\\
c_2 &= -\sum_{1\le i<j<k<n\le 6} A_{ii}A_{jj}A_{kk}A_{nn} - A_{12}A_{21}\\
&\quad \times \sum_{\substack{i<j<k\\ i,j,k\in 1,3,4,5,6}} A_{ii}A_{jj}A_{kk}\\
&\quad -A_{31}A_{13}\sum_{\substack{i<j<k\\ i,j,k\in 2,3,4,5,6}} A_{ii}A_{jj}A_{kk} - A_{34}A_{43}\\
&\quad \times \sum_{\substack{i<j\\ i,j\in 1,2,5,6}} A_{ii}A_{jj} + A_{34}A_{43}A_{21}A_{12}\\
&\quad +A_{15}A_{53}A_{31}\left(A_{22}+A_{44}+A_{66}\right) + A_{56}A_{65}A_{34}A_{43}\\
&\quad \times \sum_{\substack{i<j\\ i,j\in 1,2,3,4}} A_{ii}A_{jj}\\
&\quad +A_{56}A_{65}\left(-A_{21}A_{12}-A_{31}A_{13}+A_{34}A_{43}\right),\\
c_1 &= -A_{11}A_{22}A_{33}A_{44}\left(A_{55}+A_{66}\right)\\
&\quad -A_{11}A_{22}A_{55}A_{66}\left(A_{44}+A_{33}\right)\\
&\quad -A_{33}A_{44}A_{55}A_{66}\left(A_{22}+A_{11}\right)\\
&\quad +A_{12}A_{21}\sum_{\substack{i<j<k\\ i,j,k\in 1,3,4,5,6}} A_{ii}A_{jj}A_{kk} + A_{31}A_{13}\\
&\quad \times \sum_{\substack{i<j<k\\ i,j,k\in 2,3,4,5,6}} A_{ii}A_{jj}A_{kk} - A_{34}A_{43}A_{21}A_{12}\left(A_{55}+A_{66}\right)\\
&\quad +A_{34}A_{43}\left(A_{66}A_{11}+A_{55}A_{11}+A_{66}A_{55}A_{22}+A_{66}A_{55}A_{11}\right)\\
&\quad +A_{34}A_{43}A_{56}A_{65}\big(A_{11}A_{22}A_{33}+A_{11}A_{22}A_{44}\\
&\quad +A_{44}A_{33}A_{22}+A_{44}A_{33}A_{11}\big)\\
&\quad -A_{15}A_{13}A_{31}\left(A_{66}A_{22}+A_{44}A_{22}+A_{66}A_{44}\right)\\
&\quad +A_{56}A_{65}\big[A_{21}A_{12}\left(A_{33}+A_{44}\right)\\
&\quad +A_{31}A_{13}\left(A_{22}+A_{44}\right) - A_{34}A_{43}\left(A_{11}+A_{22}\right)\big],\\
c_0 &= +A_{11}A_{22}A_{33}A_{44}A_{55}A_{66} - A_{21}A_{12}A_{11}A_{33}A_{44}A_{55}A_{66}\\
&\quad -A_{31}A_{13}A_{22}A_{33}A_{44}A_{55}A_{66}\\
&\quad -A_{11}A_{22}A_{55}A_{66}A_{43}A_{34} - A_{11}A_{22}A_{33}A_{44}A_{43}A_{34}A_{56}A_{65}\\
&\quad +A_{22}A_{44}A_{66}A_{15}A_{53}A_{31} + A_{12}A_{21}A_{34}A_{43}A_{55}A_{66}\\
&\quad -A_{56}A_{65}\big(A_{21}A_{12}A_{33}A_{44}+A_{31}A_{13}A_{22}A_{44}\\
&\quad -A_{34}A_{43}A_{11}A_{22}\big) - A_{56}A_{65}A_{34}A_{43}A_{12}A_{21}.
\end{aligned}$$

Supposing $\lambda = \varpi^2$, the solution of Eq. (11) still has several possibilities:

(1) If $\varpi^2 = -\alpha$ ($\alpha > 0$), we obtain: $\lambda = \pm \mathrm{j}\sqrt{\alpha}$ (the imaginary solution). In this case, a Hopf bifurcation emerges in the system (or the limit cycle appears). This case corresponds to case (iii).

(2) If $\varpi^2 = \alpha$ ($\alpha > 0$), we obtain: $\lambda = \pm\sqrt{\alpha}$ (the real number solution). Responding to the case, two possibilities of dynamic behaviors are guided by stability and instability. The system moves unstably, and its equilibrium points are unstable when $\lambda = \sqrt{\alpha}$. The system moves stably, and its equilibrium points are asymptotically stable when $\lambda = -\sqrt{\alpha}$. The two cases respond to case (ii).

(3) If $\varpi^2 = \mathrm{j}\beta$ ($\beta > 0$), we obtain: $\lambda = \pm\sqrt{\beta}(\sqrt{2}+\mathrm{j}\sqrt{2})$ (the complex number solution). Responding to this case, two possibilities of dynamic behaviors are guided by stability and instability. The system moves unstably, and its equilibrium points are unstable when $\lambda = \sqrt{\beta}(\sqrt{2}+\mathrm{j}\sqrt{2})$. The system moves stably, and its equilibrium points are stable when $\lambda = -\sqrt{\beta}(\sqrt{2}+\mathrm{j}\sqrt{2})$.

(4) If $\varpi^2 = \alpha + \mathrm{j}\beta$ ($\alpha \neq 0$ and $\beta \neq 0$), Eq. (13) still has another complex number solution. We obtain the following: $\lambda = \sqrt{\alpha+\mathrm{j}\beta} = p + \mathrm{j}q$, where $p = \pm[(\alpha+\sqrt{\alpha^2+\beta^2})/2]^{1/2}$ and $q = \pm[(-\alpha+\sqrt{\alpha^2+\beta^2})/2]^{1/2}$. Responding to the case, the dynamic behavior is dominated by the value p. When $p > 0$, the system moves unstably, and its equilibrium points are unstable. When $p < 0$, the system moves stably, and its equilibrium points are stable.

3.2. Function theory

Because there is no root formula for a tri-quadratic form, using the linear stability of the equilibrium points, we investigate the root distributions and conduct an alternative qualitative analysis of the dynamics using a nonlinear function view.

In this section, we will prove the instability and multistability of each laser using a set of nonlinear algebraic equations. Setting $a_{1,2,3} = a$, $\sigma_{1,2,3} = \sigma$, $R_{1,2,3} = R$, and $m_{1,2,3} = m \neq 0$ for simplicity, the field values of the equilibrium points are obtained using the following equations:

$$m(S_{30}+S_{20}) = S_{10}\left\{1-\sigma R/\left(\sigma+S_{10}^2\right)\right\}, \quad (12)$$

$$mS_{10} = -S_{20}\left\{1-\sigma R/\left(\sigma+S_{20}^2\right)\right\}, \quad (13)$$

$$mS_{20} = S_{30}\left\{1-\sigma R/\left(\sigma+S_{30}^2\right)\right\}, \quad (14)$$

where footnote "0" indicates the field values of the equilibrium points. Subsequently, we will prove the existence of instability

and multi-stability when there are multi-solutions of systems in mathematics that correspond to the multi-valued outputs of the system in physics. On the one hand, the multi-valued outputs of the system are a key factor leading to instability. In dynamics, the system has instability. On the other hand, we note that the stable, multi-valued outputs of the system also lead to multi-stability. In dynamics, the system behaves in a quasi-periodic state and shows a quasi-periodic cycle (a quasi-periodic attractor) in its dynamic phase space. Using Eq. (12), we obtain the following equation:

$$S_{10}^3 - m\sigma(S_{30}+S_{20}) \times S_{10}^2 - \sigma(1-R) \times S_{10} - \sigma(S_{30}+S_{20}) = 0. \tag{15}$$

Setting

$$\widehat{P} = -m\sigma(S_{30}+S_{20}), \quad \widehat{Q} = -\sigma(1-R), \quad \widehat{G} = -\sigma(S_{30}+S_{20}).$$

Equation (15) can be rewritten as follows:

$$x^3 + x^2\widehat{P} + x\widehat{Q} + \widehat{G} = 0, \tag{16}$$

or

$$y^3 + 3yp + 2q = 0, \tag{17}$$

where

$$x = y - \widehat{P}/3, \quad 3p = \widehat{Q} - \widehat{P}^2/3, \quad 2q = 2\widehat{P}^3/27 - \widehat{P}\widehat{Q}/3 + \widehat{G}.$$

We discuss the three cases as follows:

(i) When $q^2 + p^3 > 0$, a real root and two complex roots are obtained by

$$y_1 = u + v, \quad y_2 = -\frac{1}{2}(u+v) + \mathrm{i}\frac{\sqrt{3}}{2}(u-v),$$
$$y_3 = -\frac{1}{2}(u+v) - \mathrm{i}\frac{\sqrt{3}}{2}(u-v).$$

where

$$u = \sqrt[3]{-q + \sqrt{q^2+p^3}}, \quad v = \sqrt[3]{-q - \sqrt{q^2+p^3}}.$$

(ii) When $q^2 + p^3 = 0$, three real roots are obtained by

$$y_1 = 2\sqrt[3]{-q}, \quad y_2 = y_3 = -\sqrt[3]{-q}.$$

(iii) When $q^2 + p^3 < 0$, three differential real roots are obtained by

$$y_1 = 2\sqrt{-p}\cos\left(\frac{\phi}{3}\right), \quad y_2 = 2\sqrt{-p}\cos\left(\frac{\phi}{3} + \frac{2\pi}{3}\right),$$
$$y_3 = 2\sqrt{-p}\cos\left(\frac{\phi}{3} + \frac{4\pi}{3}\right);$$

where

$$\cos\phi = \frac{q}{(p\sqrt{-p})}, \quad 0 < \phi < \pi.$$

The obtained solutions describe the field of laser 1, varying with the sum of the fields of lasers 2 and 3. This indicates that there are at least two solutions to laser 1 when the selection of the parameters meets conditions (ii) and (iii). Namely, the parameter region is unstable when $(q^2 + p^3) \leq 0$. There are three or at least two possible outputs (cf. Figs. 2–4). The multi-valued solutions exist in the instability region (special unstable parameter sets). Alternatively, the multi-valued outputs emerge in the physically unstable region. The instability really results in the multi-valued solutions in mathematics and the multi-valued outputs of laser 1 in physics. Equations (12) and (15) reveal the connection between multi-valued solutions and physical instability, proving instability exists for laser 1 in the unstable parameter region. Thus, we have proven that instability exists in laser 1 in the unstable parameter region.

For the same principle, using Eqs. (13) and (14), respectively, we obtain

$$S_{20}^3 + m\sigma S_{10} \times S_{20}^2 - \sigma(1-R) \times S_{20} - \sigma S_{10} = 0, \tag{18}$$
$$S_{30}^3 - m\sigma S_{20} \times S_{30}^2 - \sigma(1-R) \times S_{30} - \sigma S_{20} = 0. \tag{19}$$

In a similar analysis to Eq. (16), we can attain the following results: S_{20} has three solutions or at least two in Eq. (18), when S_{10} has a stable value. For laser 2, the multi-valued solutions readily exist in mathematics, and the multi-valued outputs of laser 2 can emerge in physics (cf. Fig. 3). Equation (18) reveals the multi-valued connection between laser 2 and laser 1 due to their coupling.

In a similar analysis to Eq. (16), S_{30} has three solutions or at least two in Eq. (19), when S_{20} has a stable value. For laser 3, the multi-valued solutions readily exist in mathematics, and the multi-valued outputs of laser 3 can emerge in physics (cf. Fig. 4). Equation (19) reveals the multi-valued connection between laser 3 and laser 1 due to their coupling.

Due to the existence of three-laser coupling, multi-valued solutions readily exist in the region of instability, and the multi-valued outputs can emerge in the corresponding physically unstable region. The instability really results in the multi-valued outputs (or the physical instability).

Equations (12)–(14) readily dominate all equilibrium points of the system, including three sets of nonlinear algebraic equations. Therefore, there is instability on each laser in the unstable parameter region when the appearance of a perturbation from the neighboring laser or the variety of the delayed time. There are always perturbations and delayed times on each subsystem of the tri-laser system, so we have proven that there is deep instability in the tri-laser system when the parameters are set in the unstable parameter region (cf. Figs. 2–4, in which the numeric result corresponds well with our theoretical analysis).

Simultaneously, we cannot point to one solution (or one equilibrium point) that is better than another solution (or an-

other equilibrium point). We deduce that dynamic behavior displays an unstable oscillation around the equilibrium points when the second oscillation of the field of one laser is continuously stimulated by another field from another laser, and the oscillation cannot lock in an equilibrium point in the unstable parameter region. In addition, instability always causes an unstable state to occur in the system when perturbation or delayed time varies. Thus, such a performance easily leads to chaos.

3.3. Strange attractor and quasiperiodic attractor

The multi-value distribution of equilibrium points in a nonlinear system may result in the appearance of a strange attractor and quasi-periodic attractor in the dynamic phase space. After inspecting the equilibrium points besides the zero solution, another set of equations describing the distribution of the field values of the equilibrium points is obtained with

$$S_{10\pm} = \pm\sqrt{\sigma\,(R/D_{10}-1)}, \tag{20}$$

$$S_{20\pm} = \pm\sqrt{\sigma\,(R/D_{20}-1)}, \tag{21}$$

$$S_{30\pm} = \pm\sqrt{\sigma\,(R/D_{30}-1)}. \tag{22}$$

From Eqs. (20)–(22), we found at least two sets of obvious solutions for the root of the field value of the equilibrium point of each laser, indicating the existence of at least two sets of equilibrium points for each laser. Accordingly, the switching behavior may be stimulated on each laser when the anti-phase coupling and the delayed time operate. In dynamics, each laser switches stochastically between its two equilibrium points because one equilibrium point cannot be supposed to have stronger dominance than another. Simultaneously, the system oscillates stochastically among its equilibrium points when the second oscillation of the field of one laser is continuously stimulated by another field from another laser. This results in the appearance of the twin-scroll strange attractor in the dynamic phase space of each laser. The tri-laser system has at least six sets of equilibrium points besides the zero solution. In dynamics, the system behaves stochastically around its equilibrium points to show instability. Consequently, the attractor in the system is characterized by full ergodicity, high complexity, and high randomness in the dynamic phase space when the parameters are set in the unstable parameter region, because the second oscillation of each laser's field is continuously stimulated by the field from the other laser. Hence, we can deduce that the six-scroll strange attractor could be illustrated in the phase space comprising S_1, S_2, and S_3 of the assembled tri-laser system under some conditions.

To verify the appearance of a strange attractor in this system, we numerically plot the moving trajectories in the dynamic phase spaces of each laser and the system (cf. Fig. 8), displaying the appearance of the twin-scroll strange attractor of each laser and the six-scroll strange attractor (a new type of hyper-scroll strange attractor) of the assembled tri-laser system. The numerical results substantiate our theory well.

Multi-stability is fascinating. Correspondingly, we lastly discuss the multi-stability of a system when a tri-laser system produces a stable multi-value output. After investigating the conclusion in Subsection 3.2 and Eqs. (20)–(22), we find the possibility for a stable multi-value output operated on the assembled tri-laser system under a parameter region. This leads to the system's moving in a stable orbit to form a set of quasi-periodic attractors visualized in the dynamic phase space (cf. Figs. 14 and 15, in which these attractors have disparate periodicities, such as the five period, six period, and seven period).

4. Numeric results and analysis

In this section, we first numerically illustrate the instability of the system using a typical nonlinear curve diagram. Second, we provide a route to chaos after bifurcation to illustrate the dynamic behavior of the system. Subsequently, chaos control is introduced. Finally, we discuss the system's output and its dynamic movement via LEs.

4.1. Instability

By numerically calculating Eq. (14), the stable output field of laser 1 varies with the sum of the stable values of lasers 2 and 3 in Figs. 2(a) and 2(b), illustrated with a typical nonlinear function curve diagram. Figure 2(a) demonstrates the existence of an instability (IS) region; there is a special parameter set (or the instability parameter region), in which there are three values of or at least two values of the field of laser 1, where the fitting normalization factors are $a = 30$, $\sigma = 0.1$, $m = 0.3$, $R_1 = R_2 = R_3 = 4$ (three subsystem lasers were set to have identical parameters).[39] Corresponding to any value $m(S_{30}+S_{20})$ in an IS region, in physics, the dynamic behavior of laser 1 stochastically moves around its three or at least two equilibrium points. It cannot be locked onto one equilibrium point to maintain stabilization because we cannot suppose that one equilibrium point is superior to another. Hence, the instability existence of the equilibrium points of laser 1 is proven in the IS region. When the parameter value R is set at 3, 5, and 7, respectively, Fig. 2(b) shows the output field of laser 1, varying with the sum of the values of lasers 2 and 3, in which three typical nonlinear function curves illustrate instability in the IS region. Subsequently, laser 1 may switch on three or two equilibrium points and depict instability when the parameters are set in the IS region. Meanwhile, the IS region is enlarged by adding pump levels.

By numerically calculating Eq. (15), the stable output field of laser 2 varying with the stable values of laser 1 is revealed in Figs. 3(a) and 3(b) with a typical nonlinear function

curve diagram, where $R_1 = R_2 = R_3 = 5$ in Fig. 3(a) and the value R is set to 2, 3, and 4, respectively, in Fig. 3(b). Typical nonlinear curves illustrate the existence of instability, and the IS region is enlarged by adding pump levels. Thus, laser 2 may randomly switch at three or two equilibrium points and behave unstably in the unstable parameter region.

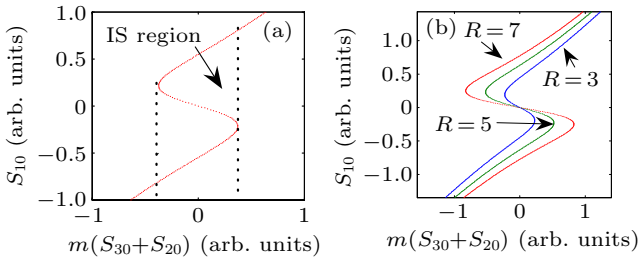

Fig. 2. Instability (IS) (a) in the system and (b) at different pump levels.

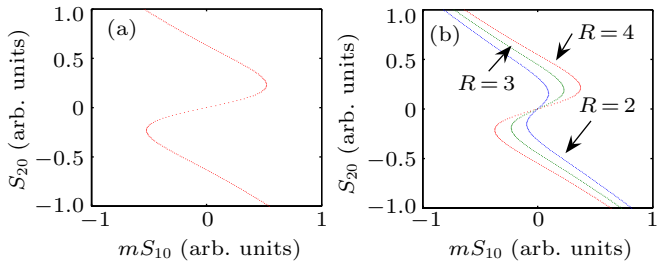

Fig. 3. Instability for (a) lasers 1 and 2 and (b) at different pump levels.

By numerically calculating Eq. (16), the stable output field of laser 3 varies with the stable values of laser 2 in Figs. 4(a) and 4(b), illustrated with a typical unstable curve diagram. There, $R_1 = R_2 = R_3 = 5$ in Fig. 3(a), and value R is set to 2, 3, and 4, respectively, in Fig. 3(b). Typical nonlinear function curves illustrate instability in the instability parameter region, where the IS region is enlarged by adding pump levels. Thus, laser 3 may randomly switch at three or two equilibrium points and show instability in the instability parameter region. Hence, the instability existence of the equilibrium points of three subsystem lasers is proven in the IS region.

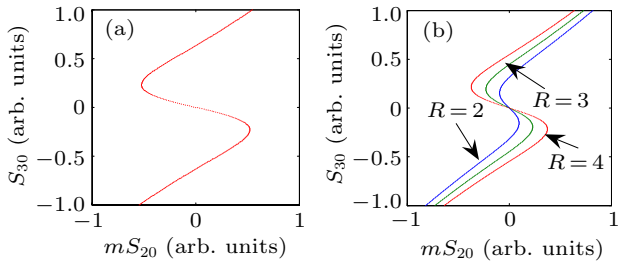

Fig. 4. Instability for (a) lasers 2 and 3 and (b) at different pump levels.

Using Figs. 3(a) and 4(a) again, we found that one laser has a stable value and another laser has three or at least two values in the instability parameter region, which implies that the system may randomly switch on equilibrium points and show instability. Hence, the existence of instability of the equilibrium points of the system is proven in the IS region.

4.2. Route to hyperchaos

In chaos research, bifurcation diagrams are often adopted to reveal the bifurcation process of dynamic systems, roughly describing their dynamic behaviors. By numerically calculating Eqs. (1)–(6), a route to chaos passing through bifurcation is depicted in Fig. 5. It visualizes the system's dynamics using the diagram of the normalized intensity $P = S^2$ versus the variation of the coupling parameter m, where the normalized parameters are $a = 30$, $\sigma = 0.1$, $R_1 = R_2 = R_3 = 4$, and $\tau = 10$. The value m shifts from 0 to 0.1 in 180 equal parts. There is a stable region from approximately 0–0.010556, a bifurcation point at 0.011111, an undamped oscillation region or a difficult-to-distinguish unstable region before 0.015, and then a chaotic region after 0.015556.

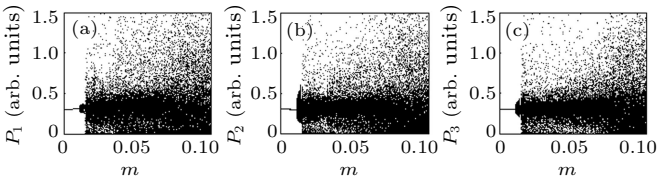

Fig. 5. Bifurcation diagram: (a) laser 1, (b) laser 2, and (c) laser 3.

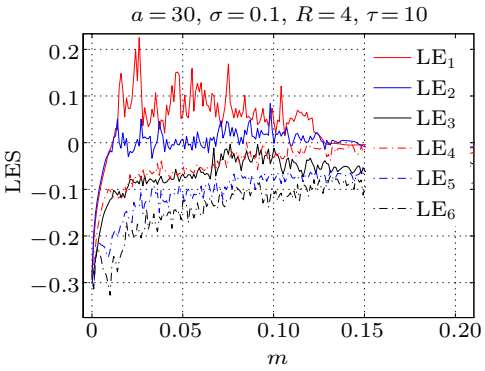

Fig. 6. The LE spectrum versus the parameter m.

A route to chaos through bifurcation was also numerically inspected and visualized by the LE spectrum. The corresponding dynamics were rigorously diagnosed using the LES. The hyperchaotic distribution in the chaotic region was divided by coupling levels. Figure 6 reveals the LE spectrum versus the parameter m. A wide chaotic region is revealed between 0.012 and 0.135, while many hyperchaotic regions are mainly distributed between 0.012 and 0.15, 0.026 and 0.032, 0.036 and 0.039, 0.07 and 0.08, 0.084 and 0.0995, 0.111 and 0.115, and 0.119 and 0.127. In these regions, the corresponding dynamics are diagnosed by the two positive LEs, and hyperchaos occurs in the laser system. Bifurcation/quasi-period occurs near 0.0114, where the maximum LE is approximately zero. This implies that the alternative appearance of those rich hyperchaotic regions results from the operation of the alternative compression and enhancement of the oscillations of neighboring lasers with different coupling levels. Thus, the structure of the tri-laser system and its anti-phase-coupling operation

readily caused the system's hyperchaos and chaos. The results demonstrate that the proposed three-laser system has the advantage of being prone to generating chaos and hyperchaos.

The dynamic behaviors of the three subsystem lasers are illustrated in Figs. 7–14, and their corresponding dynamics are rigorously diagnosed by the LEs as follows.

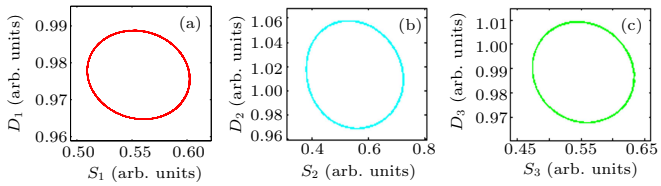

Fig. 7. Cycle one: (a) laser 1, (2) laser 2, and (c) laser 3.

Figure 7 demonstrates the limit cycle of the period 1 dynamic behavior of each laser or the three lasers pulsing at three single-periodic states when $m = 0.012$, where the leading LE is about zero. When the coupling levels are increased, the oscillations of the system are stimulated, and the second oscillation emerges. The system's behavior is developed into an undamped oscillation, and a chaotic dynamic state emerges. When $m = 0.02$ is added, Fig. 8 presents the three laser outputs and strange attractors. Figures 8(a)–8(c) reveal the undamped stochastic oscillation behaviors of the three lasers; namely, each laser displays the undamped stochastic oscillation around the equilibrium points and switches stochastically to the two equilibrium points after many undamped stochastic oscillations on one equilibrium point. Corresponding dynamic behaviors were diagnosed as chaos by their maximum LE value of 0.074. Figures 8(a)–8(c) also indicate that the wave signals from three subsystem lasers have high complicacy. We note that the waveforms in Figs. 8(a)–8(c) look like periodic digital pulses because chaos has self-similarity (or the chaotic self-similarity results in the fluctuation of the like periodic digital pulses). In fact, each pulse has a different duration and a different amplitude or waveform in their zoom. However, the system's moving phase trajectory formed a typical chaotic attractor, as displayed in Figs. 8(d)–8(f). Figure 8(d) shows the four-scroll attractor in the phase space, consisting of S_1 and S_2. Due to many undamped stochastic oscillations on one equilibrium point (cf. Figs. 8(a)–8(c)), a single scroll formed around this equilibrium point in the phase space. In the phase space of S_1 and S_2, around each equilibrium point, there is a single scroll. Due to the existence of switching (cf. Figs. 8(a)–8(c)), the four-scroll attractor formed around the four equilibrium points. Figure 8(d) also shows that the switching variation alters from above to downward or from the left to the right, stochastically rounding their four equilibrium points, namely: Dual switching occurs in two lasers, 1 and 2. Figure 8(e) shows the four-scroll attractor in the phase space of S_2 and S_3. Figure 8(f) reveals the four-scroll attractor in the phase space of S_1 and S_3. Hence, in the phase space consisting of S_1, S_2, and S_3, we can deduce that the six-scroll attractor will form around the six equilibrium points of the system. Figure 8(g) obviously depicts the chaotic six-scroll attractor in the phase space consisting of S_1, S_2, and S_3, where three scrolls are distributed in a triangle in the top part and three scrolls are distributed in a triangle in the lower part, where the moved trajectory of the system results from the system's moving stochastically and endlessly around the six equilibrium points. The system exhibits a new type of six-scroll attractor, a new type of hyperstrange attractor. For most laser systems, it is difficult to find the chaotic six-scroll attractor that originally existed in such a tri-laser system. This indicates that this tri-laser system has the advantage of forming chaotic six-scroll attractors or a new type of hyperstrange attractor.

When the coupling levels are increased, the second oscillations of each subsystem laser are generally enhanced, and switching is basically produced, leading to fully developed chaos and hyperchaos. When $m = 0.039$, Fig. 9 shows the hyperchaotic six-scroll attractor, and the corresponding dynamic behavior is diagnosed as hyperchaos by its two positive LEs of 0.048 and 0.015. Clearly, the hyperchaotic six-scroll attractor in dynamics has higher complexity and randomness than a single-scroll attractor or double-scroll attractor.

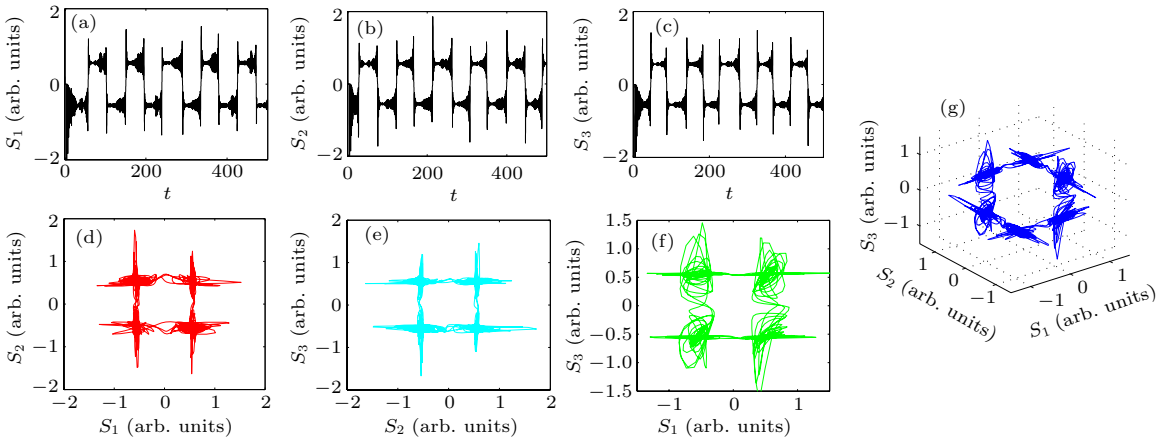

Fig. 8. Each laser output and its strange attractor. (a) Laser 1, (b) laser 2, (c) laser 3, (d) four-scroll attractor in a phase space consisting of S_1 and S_2, (e) four-scroll attractor in a phase space of S_2 and S_3, (f) four-scroll attractor in a phase space of S_1 and S_3, and (g) six-scroll attractor in a phase space consisting of S_1, S_2 and S_3.

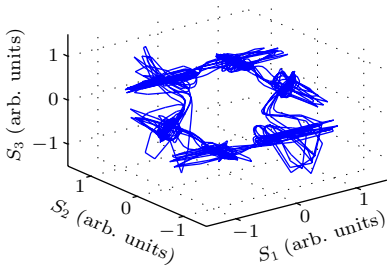

Fig. 9. The hyperchaotic six-scroll attractor.

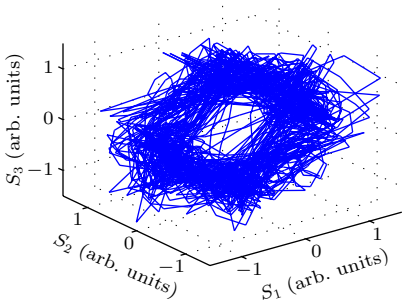

Fig. 10. Another hyperchaotic attractor.

When the coupling levels are further increased, the stochastic oscillation of the system is stimulated, and the second oscillation is enlarged again. The system is developed into an enhanced undamped oscillation, which results in another fully developed hyperchaotic dynamic state emerging in the system. When $m = 0.099$, Figs. 10–12 show the multi-scroll hyperchaotic attractors in the system, and the corresponding dynamic behaviors are diagnosed as hyperchaos by the two positive LEs of 0.07 and 0.04. Figure 10 reveals roughly the six-scroll hyperchaotic attractor in a phase space consisting of S_1, S_2, and S_3, in which the moved trajectory of the system results from the system's moving endlessly around the six equilibrium points. The hyperchaotic six-scroll chaotic attractor is characterized by full ergodicity, high complexity, and high randomness. For most laser systems, such a six-scroll attractor is difficult to create; it is only found in this laser system. Figures 11(a) and 11(b) show obviously different four-scroll attractors, where Fig. 11(a) shows a four-scroll attractor in a phase space consisting of S_1 and S_2. Figure 11(b) illustrates another four-scroll attractor in the S_2 and S_3 phase space, and Fig. 11(c) demonstrates roughly a four-scroll attractor in the phase space of S_1 and S_3. Figures 12(a)–12(c) display the waveform of each laser, and Figs. 12(d)–12(f) depict the double-scroll attractor of each laser. From the listed results, it was found that each laser maintained its nature. However, the built-up system shows a new type of hyperchaotic four-scroll attractor and hyperchaotic six-scroll attractor. These figures reveal that the movement around the equilibrium points gives the attractor full densification and high complexity. Hence, these hyperchaotic attractors in dynamics are deeply characterized by full ergodicity, high complexity, and high randomness. If this system is used in chaotic cryptography, it will enhance encoding security.

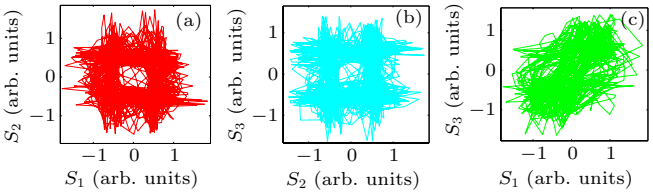

Fig. 11. Hyperchaotic attractors.

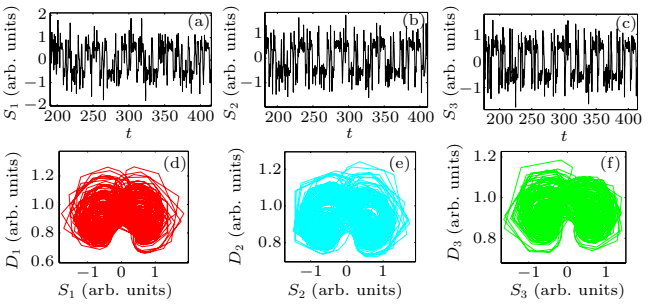

Fig. 12. Hyperchaotic waveform and attractor in each laser.

Under distinct delayed times ($\tau = 2$), Fig. 13 shows the LE spectrum versus the parameter value m. The two chaotic regions are mainly distributed from 0.015 to 0.06 and from 0.074 to 0.16. The hyperchaotic region is mainly distributed between 0.02 and 0.038, the quasi-periodic regions are mainly distributed between 0.06 and 0.09, and the stable region is distributed between 0 and 0.01. The result proves that the distinct delayed times change the behavior of the system; chaos and hyperchaos still appear.

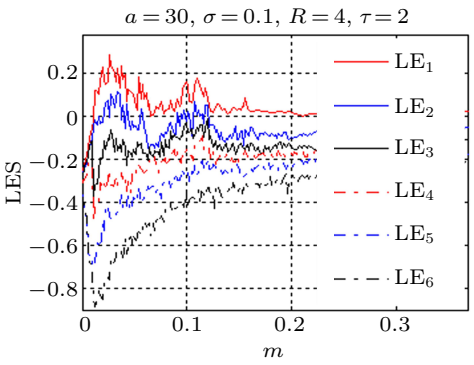

Fig. 13. The LE spectrum versus the parameter m.

4.3. Chaos control: Control of a route away from chaos

Chaos control is another important issue in chaos.[31–33] Chaos control indicates that a chaotic movement can be suppressed to reduce it to a quasi-periodic state or a stable state. For the chaos control of lasers, various control methods were presented, such as current modulation, optic feedback, dual feedback, photoelectric feedback, wedge feedback, and external optic injection.[29,34] Here, the parameter method of chaos control is used. For this three-laser system, coupling dominates the dynamic behavior of the system. Its parameter value

m represents the injection level from one laser to another, symbolizing the coupling level of the three lasers. Therefore, we chose parameter m as the control parameter. In practice, we can adopt optic amplifiers to shift the injection level into each laser or adopt optic attenuators to shift light's quantity through optic attenuators to adjust the injection level into each laser. Adjusting the parameter value m, we achieve chaos control of the chaotic system and give our chaos control result: the control of a route away from chaos passing through a quasi-period, such as period-three, period-five, period-six, and period-12, as exhibited in Fig. 14, when $\tau = 1$ and the other parameters correspond to the case of Fig. 12. Figures 14(a)–14(f) visualize the controlling of a route away from chaos: chaos (the maximum LE1 = 0.258) when the control parameter keeps on $m = 0.03$, six cycles (LE1 = 0) when the control parameter shifts on $m = 0.04$, five cycles (LE1 = 0) when adjusting $m = 0.05$, three cycles (LE1 = 0) when adjusting $m = 0.07$, another five cycles (LE1 = 0) when adding $m = 0.09$, and 12 cycles (LE1 = 0) when $m = 0.12$, respectively. Hence, we revealed the hidden behavior of the system, and chaos control has been successfully achieved. The produced quasi-periodic attractors play up our interests quite well.

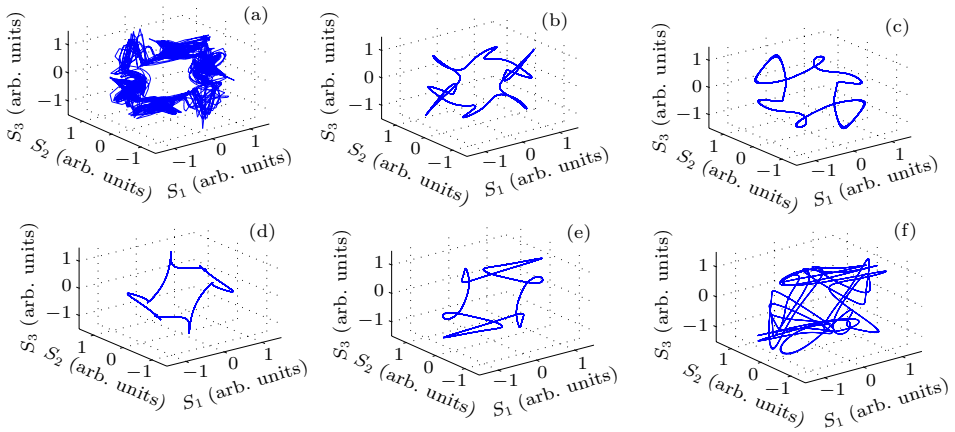

Fig. 14. The control of a route away from chaos passing through a quasi-period. (a) Chaos for $m = 0.03$, (b) six cycles for $m = 0.04$, (c) five cycles for $m = 0.05$, (d) three cycles for $m = 0.07$, (e) another five cycles for $m = 0.09$, and (f) 12 cycles for $m = 0.12$.

4.4. Chaos control: Delayed time leads to a route to hyperchaos

Subsequently, we numerically examine the bifurcation processes occurring in the laser system and analyze the stability of the limit cycles embedded in the phase space along the route to chaos and hyperchaos using the bifurcation diagram and the LE spectrum, which can be guided by the delayed times in Figs. 15 and 16. Of course, we are particularly interested in understanding how a typical bifurcation diagram develops in terms of delayed times. We watch the main features in terms of the delayed times in Fig.15: stability, the bifurcation point, the period, and the sudden transition to chaos. Figure 16 is used to numerically inspect the bifurcation processes according to the LE spectrum. (The maximum LE is LE_1, and the second LE is LE_2.) The main features of the delayed times show stability ($LE_1 < 0$), period bifurcation ($LE_1 = 0$), the sudden transition to chaos ($LE_1 > 0$), and hyperchaos ($LE_1 > 0$ and $LE_2 > 0$). The clear repetitive structure of this LE spectrum is a numeric indication of the property of the period-bifurcation dynamics in the system. The LE values were altered at different delayed times. Both results prove that bifurcation processes are very much guided by various delayed times. These results corroborate the conclusion (iii) of Eq. (20). In physics, the results also revealed that the alternative appearance of chaos and hyperchaos results from the operation of the alternative compression and the enhancement of the oscillations of neighboring lasers with various delayed times. Therefore, the structure of the tri-laser system, the delay time, and the anti-phase coupling effect jointly determine the dynamic characteristics of the system, leading to state changes in the system and the appearance of chaos and hyperchaos.

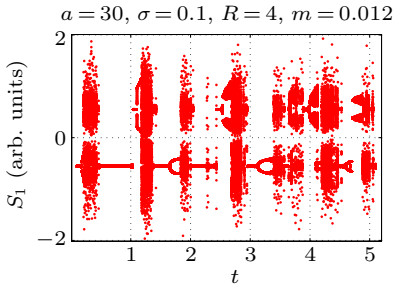

Fig. 15. The bifurcation diagram.

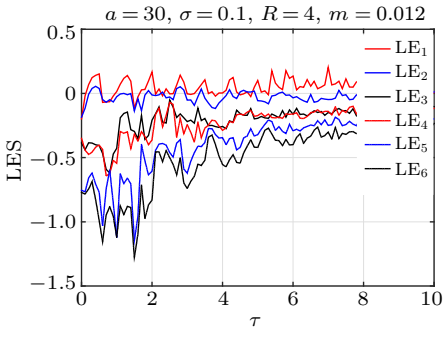

Fig. 16. The LE spectrum diagram.

5. Conclusion

This paper studied routes to chaos and hyperchaos after the quasi-periodic bifurcation of the class B tri-laser system. We introduced its technical scheme and theoretical model within laser physics and nonlinear dynamics. We qualitatively analyzed the dynamic behavior of the system. We numerically offered bifurcation processes guided by delayed times and provided zones of hyperchaotic distribution in the chaotic region based on feedback levels. We expounded on how both delayed time and anti-phase-coupling effects impact the tri-laser system's behavior and lead to chaotic and hyperchaotic phenomena. Our analysis helps reveal the system's sensitivity to the structural factors of the tri-laser system and offers a deeper understanding of stochastic behavior. Our research not only reveals the behavior of the system under different conditions but also the stability of the three-laser system and the occurrence of bifurcation phenomena. The investigation of the tri-laser configuration (or high-order nonlinear systems) is of great significance, providing insights into the tri-laser structure that plays a special role in the chaotic system.

Instability was forecast in theory, while our numerical simulation demonstrated the existence of instability via a typical unstable curve diagram, in which the instability region was found to be enlarged by adding pump levels. The system showed some typical nonlinear dynamic behaviors, such as hyperchaos, chaos, and period 1, as well as coexistent scenarios, and exhibited a route to hyperchaos after passing bifurcation. Interestingly, the dynamic movement of the tri-laser system shows almost no end, no rules, and randomness. The chaotic and hyperchaotic behaviors and their distribution regions are obviously indicated by their LE spectra. Their four-scroll strange attractor and six-scroll strange attractor dynamics are characterized by full ergodicity, high complexity, and high randomness. The numerical results are consistent with our theory. Multi-stability was studied to show multi-periodic attractors. The rich dynamic behaviors of the system and many paths to chaos and hyperchaos were revealed. Chaos control is operated and successfully achieved, which plays up our interest quite deeply. We found that the structure of the tri-laser system, the delay time, and the anti-phase coupling effect jointly determine the dynamic characteristics of the system, leading to state changes in the system and the appearance of chaos and hyperchaos. The system shows the strong ability to form a new type of multi-scroll attractor and has the advantage of forming a new type of hyperstrange attractor. The proposed three-laser system obviously has the advantage of being prone to generating chaos and hyperchaos. If used for secure communications, its security would be enhanced. The tri-laser system and its dynamics are valued for the study of laser hyperchaos and multi-body optic problems. We adopted nonlinear function theory to reveal the instability of the system. It also provides a significant reference for studying dynamic systems described by differential equations of high degree. The result has a reference value for a chaotic transmitter, laser technology, hyperchaos, and their applications.

Acknowledgements

This work is supported by Key Subjects of Jiangsu Province and Nanjing, and the Nanjing Key Laboratory, China.

References

[1] Chai M M, Qiao L J, Li S H, Wei X J, Xu H C, Zhao J and Zhang M J 2022 *J. Lighwave Technol.* **40** 5952
[2] Esqueda de la Torre J O, García-López J H, Jaimes-Reátegui R, Huerta-Cuellar G, Aboites V and Pisarchik A N 2023 *Photonics* **10** 813
[3] Kingston S L, Balcerzak M, Dana S K and Kapitaniak T 2023 *Chaos* **33** 023128
[4] Harayama T, Sunada S, Yoshimura K, Davis P, Tsuzuki K and Uchida A 2011 *Phys. Rev. A* **83** 031803
[5] Zhang J Z, Wang A B, Wang J F and Wang Y C 2009 *Opt. Exp.* **17** 6357
[6] Sciamanna M and Shore K A 2015 *Nat. Photonics* **9** 151
[7] Zhang W L, Pan W, Luo B, Li X F, Zou X H and Wang M Y 2007 *J. Opt. Soc. Am. B* **24** 1276
[8] Fu Y, Cheng M, Jiang X, Deng L, Ke C, Fu S, Tang M, Zhang M, Shum P and Liu D 2018 *Nonlinear Dyn.* **94** 1949
[9] Li Q, Chen D, Bao Q, Zeng R and Hu M 2019 *Appl. Opt.* **58** 1715
[10] Al Bayati B M, Ahmad A K and Al Naimee K A M 2018 *J. Opt. Soc. Am. B* **35** 918
[11] Wu J, Wu Z, Liu Y, Fan L, Tang X and Xia G 2013 *J. Lightwave Technol.* **31** 461
[12] Lawrance A J, Papamarkou T and Uchida A 2017 *IEEE J. Quantum Electron.* **53** 8000210
[13] Jiang N, Xue C, Liu D, Lv Y and Qiu K 2017 *Opt. Lett.* **42** 1055
[14] Yi L, Ke J, Xia G and Hu W 2018 *J. Opt.* **20** 024004
[15] Xue C P, Xia Y K, Chen W, Gu P and Zhang Z 2023 *Opt. Lett.* **48** 2611
[16] Ke J, Yi L, Xia G and Hu W 2018 *Opt. Lett.* **43** 1323
[17] Yan S L 2012 *Opt. Laser Technol.* **44** 83
[18] Wang A B, Wang Y C and Wang J F 2009 *Opt. Lett.* **34** 1144
[19] Hegarty S P, Goulding D, Kelleher B, Huyet G, Todaro M T, Salhi A, Passaseo A and Vittorio M D 2007 *Opt. Lett.* **32** 3245
[20] Wunsche H J, Bauer S, Kreissl J, Ushakov O, Korneyev N, Henneberger F, Wille E, Erzgraber H, Peil M, Elsaesser W and Fischer I 2005 *Phys. Rev. Lett.* **94** 163901
[21] Hill M T, de Waardt H and Dorren H J S 2001 *IEEE J. Quantum Electron.* **37** 405
[22] Hill M T, Dorren H J S, de Vries T, Leijtens X J M, den Besten J H, Smalbrugge B, Oei Y S, Binsma H, Khoe G D and Smit M K 2004 *Nature* **432** 206
[23] Mohrle M, Sartorius B, Bornholdt C, Bauer S, Brox O, Sigmund A, Steingruber R, Radziunas M and Wunsche H J 2001 *IEEE J. Sel. Top. Quantum Electron.* **7** 217
[24] Hong Y H 2015 *IEEE J. Sel. Top. Quantum Electron.* **21** 1801007
[25] Yan S L 2023 *J. Optical Commun.* **44** 673
[26] Yan S L 2024 *Electron. Lett.* **60** e70119
[27] Huerta-Cuellar G, Pisarchik A N and Barmenkov Y O 2008 *Phys. Rev. E* **78** 035202
[28] Pisarchik A N and Feudel U 2014 *Phys. Rep.* **540** 167
[29] Yan S L 2025 *Opt. Commun.* **577** 131338
[30] Yan S L 2021 *J. Optical Commun.* **42** 9
[31] Kumar G and Vijaya R 2017 *J. Opt. Soc. Am. B* **34** 574
[32] Yan S L 2025 *Opt. Commun.* **585** 131850
[33] Ott E, Grebogi C, Yorke J A 1990 *Phys. Rev. Lett.* **64** 1196
[34] Yan S L 2009 *J. Mod. Opt.* **56** 539
[35] Xue C P, Wang X, Zheng L K, Zhang H Y, Hong Y H and Zhang Z X 2025 *Chin. Phys. B* **34** 030504
[36] Wang D M, Lei Y H, Shi P F and Li Z A 2023 *Chin. Phys. B* **32** 090505
[37] Yang Y J, Liu L W, Yu L C, Kong W Z, Jiao H Y, Deng X Y and Li X Y 2025 *Chin. Phys. B* **34** 080503
[38] Jiang N, Liu D, Zhang C and Qiu K 2013 *IEEE Photon. Technol. Lett.* **25** 1912
[39] Zhang H J 1997 *Optical Chaos* (Shanghai: Shanghai Scientific and Technological Education Publishing House)